International Journal of Fatigue 135 (2020) 105530

Contents lists available at ScienceDirect

International Journal of Fatigue

journal homepage: www.elsevier.com/locate/ijfatigue

Experimental and numerical study of mooring chain residual stresses and implications for fatigue life

Ershad P. Zarandi*, Bjørn H. Skallerud

Department of Structural Engineering, Norwegian University of Science and Technology (NTNU), Richard Birkelands vei 1A, 7491 Trondheim, Norway

ARTICLE INFO

Keywords:
Residual stress
Neutron diffraction
Hole drilling
Finite element analysis
Crack initiation life estimation

ABSTRACT

Residual stresses in large mooring chains were measured for the first time in this study. Two measurement techniques were employed (neutron diffraction and hole drilling). Elastic-plastic finite element simulation of the proof loading was conducted, and the computed residual stresses were compared to the experimental measurements. Further, the cyclic plasticity of the material was taken into account to investigate residual stress redistribution caused by introduction of corrosion pits and cyclic service loads. A critical damage parameter was employed to estimate fatigue crack initiation life of corroded mooring chains subjected to various service load levels considering the effect of residual stresses.

1. Introduction

Sources of energy at sea and under the seabed have captured engineers' attentions from onshore to offshore productions in the past few decades. Accordingly, the number of the offshore production storage and offloading system has increased [1]. However, the uninterrupted operation of these offshore facilities necessitates the integrity of their mooring systems that hold these facilities in position during an operation when subjected to dynamic loads from wind, wave, and current as well as a continuous exposure to a corrosive environment. A single line failure increases the load level on the adjacent lines that may cause failure in them resulting in the operation shutdown, pollution, material loss and risking human life. The high rate of failure of offshore mooring chains demands enhanced understanding of the phenomena correlated to the fatigue life of these chains, e.g. residual stresses (RS) and corrosion, to improve their design and enhance their reliability against failure [1–3].

To assure the strength capability of mooring chains, offshore industry standards (e.g. see [4,5]) require mooring chains to be proof load (PL) tested before being installed offshore. The test involves axially loading the chain up to 70% of its minimum breaking load (MBL) resulting in extensive plastic deformation and high RS in the chain links. To date, the offshore industry standards lack the consideration of the effects of PL level and material grade on fatigue life of different size mooring chains. The characterization of RS is essential as they directly affect the fatigue strength of materials by being added to the cyclic service stresses and act similarly as mean loads [6]. Finite element simulation of the PL test reveals that the predicted RS is highly dependent on the employed material model, chain dimensions, and PL level [7]. However, the results have not been validated experimentally.

Large-scale fatigue tests on new and used mooring chains in simulated seawater have been conducted in the past years, see e.g. [4,8,9]. However, little attention has been paid to characterizing the RS in the mooring chains. Dang Van fatigue criterion has been employed for lifetime estimation of non-corroded mooring chains [10]. Conservative predictions due to high compressive hydrostatic stress existing in the critical points were obtained for a typical studless chain link. Generally, an improved damage model combined with little knowledge of actual RS is sub-optimal and does not bring the fatigue assessment methodology much further. Hence, providing quantitative information on RS in safety-critical components such as mooring chains is of high technical value.

Several investigations have indicated the significance of corrosion on mooring chains fatigue life [11,12]. The formation of small corrosion pits that can act as stress raisers at the chain link surface results in the reduction of the chain fatigue life [13,14]. Numerical investigations have been carried out on flat and cylindrical specimens employing elastic-plastic material models as well as experimental observation to determine strain localization and elastic-plastic stress distribution around critical pits and their transition into cracks [15–19]. Although the global RS distribution might not change significantly in the chains due to corrosion, the local RS distribution around corrosion pits dramatically changes as a result of plastic straining around pitting holes, and influence pit to crack transition and the crack growth. Therefore,

* Corresponding author.
E-mail address: ershad.p.zarandi@ntnu.no (E.P. Zarandi).

https://doi.org/10.1016/j.ijfatigue.2020.105530
Received 27 September 2019; Received in revised form 2 February 2020; Accepted 4 February 2020
Available online 05 February 2020

the knowledge of current RS state is of great importance and can be obtained knowing the material's cyclic plastic properties. Further, knowledge of the initial RS state is essential for the prediction of the RS redistribution over the chain service life.

To date, no RS measurement has been carried out on large-scale mooring chains. In this study, the hole-drilling (HD) technique has been used to measure RS close to the surface of mooring chains, though, the curved surface of the chains as well as corrosion pits made the application of the HD technique challenging. Additionally, neutron diffraction (ND), a non-destructive technique indifferent to surface finish that can provide tri-axial through-depth measurements including RS gradients, has been employed for deeper measurements. Two chain links with the same size and material, one only subjected to proof load and no cyclic service loads and the other exposed to service loads as well as the proof load, were selected for the experiment to investigate RS changes after several years of service. The experimental measurements are compared with the RS predicted by finite element modeling (FEM) of proof loading. Further, the cyclic plasticity of the material is taken into account to investigate RS redistribution caused by local corrosion pits and cyclic service loads. The Fatemi-Socie multiaxial damage parameter [20] combined with Roessle-Fatemi hardness method [21] is employed to estimate fatigue crack initiation life of corroded mooring chains at various service load levels considering the effect of RS. The estimated lives were compared with experimental lives obtained from large-scale fatigue tests.

2. Methodology

2.1. Material and experimentation details

Two mooring chain links with 114 *mm* nominal diameter (D) and made of steel grade R4 have been selected for the RS measurements. The links were made by the same manufacturer following the same manufacturing procedure (welding, heat treatment, and proof loading), thus, it can be assumed that RS in both links right after production were identical. One link had been exposed to the sea loads for 18 years prior to the experiment. The link, which is here referred to as the used link, had some corrosion evidence at the surface. The other link was 10 years old at the time of the experiment but had never been exposed to any cyclic service loads, as it was laid on the vessel's deck during its service life. The link, which is here referred to as the unused link, has a relatively smooth surface – close to its initial as-produced surface. The chosen links are pictured in Fig. 1. The monotonic mechanical material properties of the tested chain material are provided in [19] and listed in Table 1.

Table 1
Mechanical material properties of the mooring chain steel grade R4.

Elasticity modulus ($\boldsymbol{E}$)	[GPa]	207
True yield stress ($\boldsymbol{R_{p0.2}}$)	[MPa]	843
True ultimate stress ($\boldsymbol{R_m}$)	[MPa]	1010
Total extension at maximum force ($\boldsymbol{A_{gt}}$)		0.071
Area reduction		0.68
Poisson's ratio		0.3
Average hardness	[HB]	300

Several locations on each link were specified for the RS measurements; one at the middle of the bent part (known as the chain crown) that is recognized as the most critical location from the fatigue viewpoint [9] and the others at the straight parts to compare RS in the base and weld material. Marking of the measuring locations on the links was rather convenient enabling a point-to-point comparison between the two links and FE simulations. The measurement paths are illustrated in Fig. 2. Local cylindrical coordinate systems at every location are defined such that radial stresses are along the R-axis, hoop stresses along the θ-axis, and longitudinal stresses along the Z-axis. Considering the geometry of the chains and loading conditions, it is assumed that these axes are principal axes.

2.2. Residual stress measurement techniques

2.2.1. Neutron diffraction

Neutron diffraction technique has proven to be a useful tool in characterizing subsurface RS of metallic materials [22–25]. In this approach, the lattice spacing, which works as an atomic strain gage, of the stressed material is compared to that of a stress-free sample made from the same material providing the locked strain in the bulk material. Assuming that the measurement axes are aligned with the principal axes, using Hooke's law, and the measured strains (ε), one can calculate the RS as follows:

$$\varepsilon_i = (d_i - d_0)/d_0,\ i = r, \theta, Z$$
$$\sigma_i = \frac{E}{1+\nu}\left[\varepsilon_i + \frac{E}{1-2\nu}(\varepsilon_r + \varepsilon_\theta + \varepsilon_z)\right] \quad (1)$$

where d_0 denotes the average value of the lattice spacing of the stress-free crystalline material and d_i are the lattice spacings of the stressed

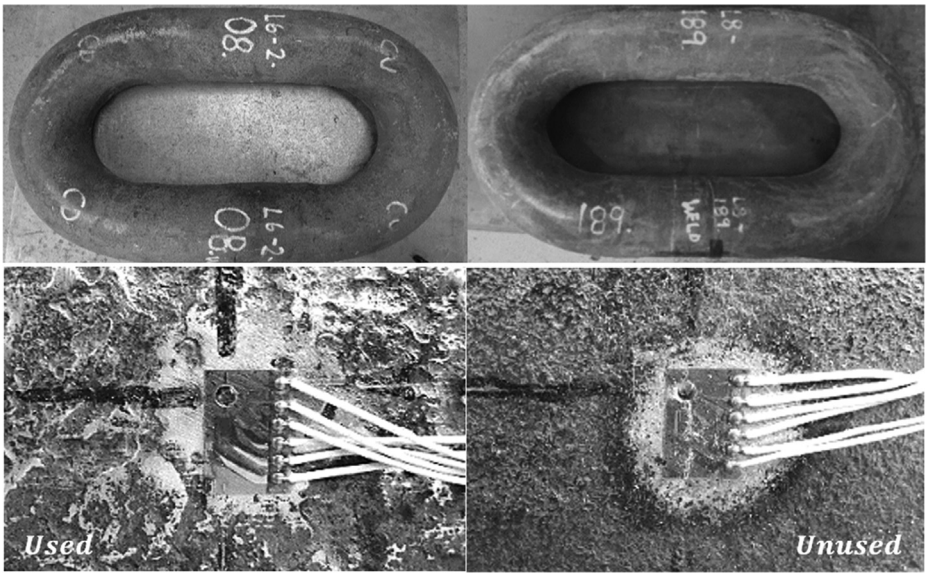

Fig. 1. Chain links chosen for the experiments and the surface condition around the measurement points at the crowns using the HD technique.

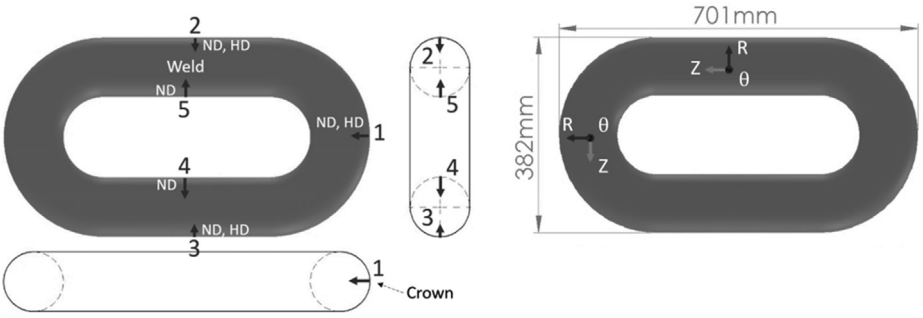

Fig. 2. Schematic of the tested chain links and the measurement paths (ND: neutron diffraction, HD: hole drilling).

material along the three perpendicular measurement axes. E denotes the material's Young's modulus, ν is the Poisson's ratio. It is worth noting that unlike the HD technique, the ND technique can provide a 3D characterization of the RS state in the material.

In the first part of the experimental work, deeper RS measurements at the specified locations on the links using this technique was carried out at STFC Rutherford Appleton Laboratory. The experiment was conducted using ENGIN-X, a 50 m flight path instrument. To obtain 3D RS, the heavy chain links (130Kg each) had to be positioned in various orientations, as in each orientation only the lattice spacing along two perpendicular axes could be measured. To facilitate this challenging task, wooden frames were designed for the links when sitting on the rotatable/movable table in ENGIN-X. The experimental setup is illustrated in Fig. 3. A 4x4x4mm gauge volume was used to enable measurements further below the surface at a reasonably short time considering the limited beamtime access and neutrons' maximum penetration capability into steels. To ensure complete filling of the gage volume in the material, the center of the gage volume was precisely positioned 3 and 4 mm below the surface using theodolites. Small T-shape samples were cut from the straight parts (both the welded side and non-welded side) of the neighboring chain link to the unused chain link and used to identify the lattice spacing of the stress-free material (d_0). The above-mentioned setup provided the RS at 3 and 4 mm below the surface.

2.2.2. Hole drilling

In this technique, after preparing the specimen surface, a small hole is drilled/milled incrementally into the material at the center of the strain rosette that is glued to the specimen. The released strains at each increment are measured by the strain gauges. The RS are calculated utilizing the measured released strains and Hooke's law. Assuming a non-uniform stress profile through the hole in thick workpieces as:

$$\begin{aligned} p_j &= (\varepsilon_3 + \varepsilon_1)_j/2P = -\tfrac{E}{1+\nu}\tfrac{\Sigma(\bar{a}\bullet p)}{\bar{a}^2}(\sigma_x)_j = P_j - Q_j \\ q_j &= (\varepsilon_3 - \varepsilon_1)_j/2Q = -E\tfrac{\Sigma(\bar{b}\bullet q)}{\bar{b}^2}(\sigma_y)_j = P_j + Q_j \\ t_j &= (\varepsilon_3 + \varepsilon_1 - 2\varepsilon_2)_j/2T = -E\tfrac{\Sigma(\bar{b}\bullet t)}{\bar{b}^2}(\tau_{xy})_j = T_j \end{aligned} \quad (2)$$

where j refers to the sequential numbers of the hole depth steps, ε_1, ε_2, and ε_3 are measured along the three in-plane axes of the attached strain gages. $\bar{a}$ is the calibration constant for isotropic equibiaxial stress (P) and $\bar{b}$ is the calibration constant for 45° shear stress (Q) and xy shear stress (T) respectively and tabulated for various hole depths in ASTM E837-13a [26]. It is worth noting that, using this technique, only a 2D stress state can be characterized and the RS along the axis normal to the surface is assumed to be zero through the depth of the hole.

In the second part of the experimental work, the RS at and close to the outer surface of the chain links were measured using this technique at SINTEF in Trondheim. A thin layer of the rust on the surface was removed using very fine Scotch-Brite surface conditioning discs. The strain rosette type 1-RY61-1.5/120 K connected to an electronic measuring system (Spider8) was used to record the strain variation during incremental hole milling using the MTS-3000 instrument. The instrument is equipped with an air turbine enabling the end mill to spin at a speed of 400000 rpm to avoid the introduction of RS during the milling process [27]. The end mills used in the experiment are inverted truncated-cone shaped with flat ends (1-SINTCTT/1), with a maximum shank diameter of 1.60 mm. The above-mentioned setup has provided the measurement of RS at a distance of up to 1 mm below the surface.

2.3. Fatigue life calculation

The Fatemi-Socie multiaxial damage parameter [20] combined with Roessle-Fatemi hardness method [21] has been employed to estimate crack initiation life of corroded mooring chains considering the present triaxial stress state and RS effect. Using this multiaxial strain-stress based critical plane approach, satisfactory fatigue life estimations were

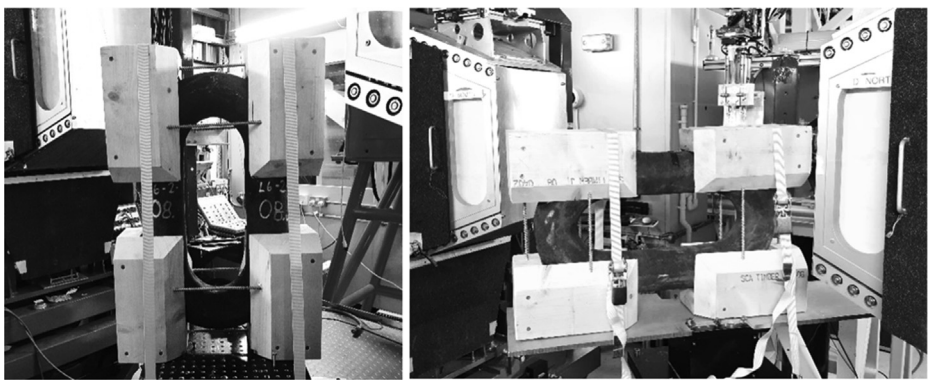

Fig. 3. The ND experimental setup at ENGIN-X.

obtained for a wide range of steels and loading conditions [28,29]. The maximum shear strain amplitude ($\Delta\gamma_{max}/2$) as the primary parameter driving the crack and the maximum normal stress acting on the maximum shear strain plane ($\sigma_{n,max}$) as the secondary parameter are related to the fatigue life (N_f) as:

$$\frac{\Delta\gamma_{max}}{2}\left(1 + k\frac{\sigma_{n,max}}{R_{p0.2}}\right) = [A(2N_f)^{-0.09} + B(2N_f)^{-0.56}][1 + kC(2N_f)^{-0.09}]$$
$$k = [0.0003(HB) + 0.0585](2N_f)^{0.09} \quad (3)$$

where $R_{p0.2}$ is the material's yield stress, A, B, and C are parameters given as a function of the material's Brinell hardness (HB, see Table 1):

$$A = \frac{5.53(HB) + 293}{200000},\ B = \frac{0.48(HB)^2 - 731(HB) + 286500}{200000}$$
$$C = \frac{1}{0.0022(HB) + 0.382} \quad (4)$$

3. Experimental results

The data presented in this section is provided in details in [30].

3.1. Measurements at the crown

The RS at the crown of the chain links have been measured and the results are presented in Fig. 4. It is seen that:

- The RS in all measurement directions are compressive in both links except the hoop RS measured by HD technique.
- The radial RS are approximately 1/4 of the longitudinal RS, which are the largest in magnitude at this region. The radial RS cannot be measured by the HD technique.
- The hoop RS measured by the ND technique are about 1/3 of the longitudinal RS.
- Using the ND technique, the RS gradients in the used chain link are opposite to that in the unused link in all measurement directions. That is, RS tends decrease with depth for the unused chain and increase with depth for the used chain. For shallower depths with the HD technique, the two links show the similar gradients with slightly lower RS in the unused link.

The last observation can be caused by the material removal at the chain surface due to the corrosive environment (in the form of corrosion pits, as seen in Fig. 1) and the cyclic straining as a result of cyclic service loads intensified by the stress concentration factor at the pit site. This results in the redistribution of RS in the material near the surface.

3.2. Measurements at the straight part (welded side)

The RS measured at location 2 on the straight part (welded side) of the links are presented in Fig. 5. It is seen that:

- The RS are compressive in all three measurement directions in both chain links.
- The hoop RS gradient obtained by the HD technique on the used link is opposite to that on the unused link.
- The radial RS measured by the ND technique is about 1/2 of the longitudinal RS and almost of the same order as the hoop RS.

Due to the beamtime access limitation, in this location, the calculation of the RS in the ND technique is based on a 2-axis measurement (hoop and longitudinal) and thus, the radial strain was set to zero when calculating RS using Eq. (1).

Fig. 6 presents the measured RS at the inside of the weld region (location 5). The application of the HD technique in this location was not possible due to limited space between the two straight parts of the links. It is seen from Fig. 6 that:

- The measured RS are compressive in all directions in both chain links.
- The radial RS are approximately 1/3 and the hoop RS are about 1/2 of the longitudinal RS.
- The near-surface RS on the used link are smaller.
- The stress gradients on the used and unused chains follow a similar trend (increasing in magnitude by depth), however, the stress gradients in the used link (almost −200 MPa/mm in all 3 directions) are steeper than that in the unused link.

3.3. Measurements at the straight part (non-welded material)

The RS measured at location 3 on the straight part (non-welded side) of the links are presented in Fig. 7. It is seen that:

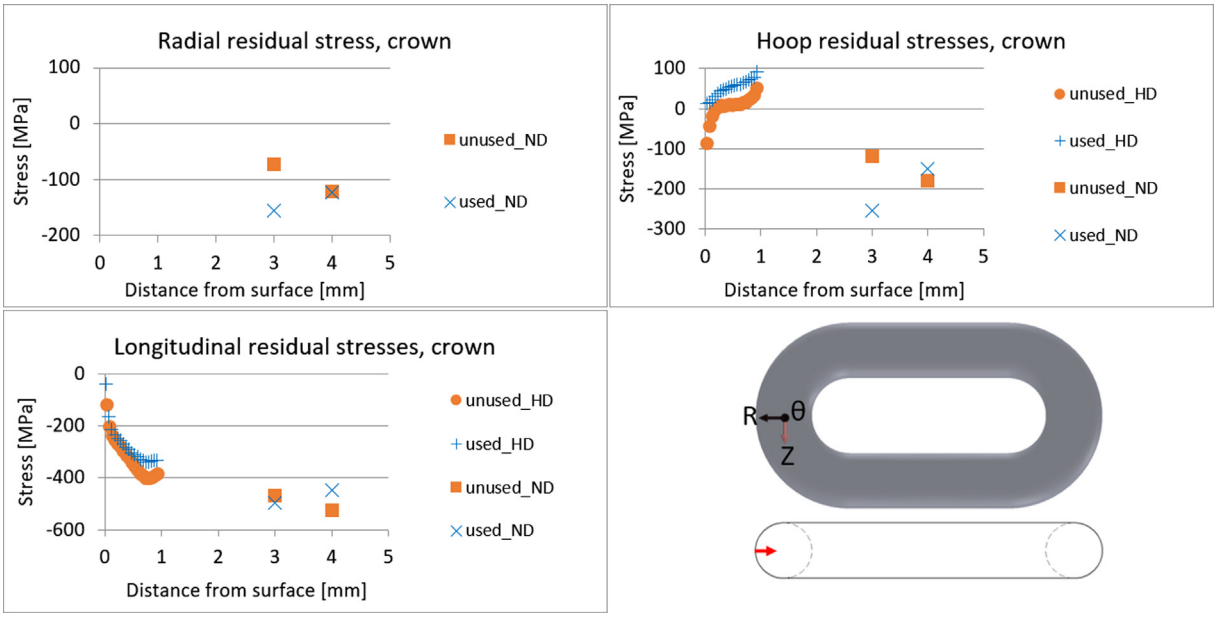

Fig. 4. Comparison of residual stresses measured at the chains' crowns (location 1) using the HD and ND techniques respectively; the red arrow indicates measurement location. (For interpretation of the references to colour in this figure legend, the reader is referred to the web version of this article.)

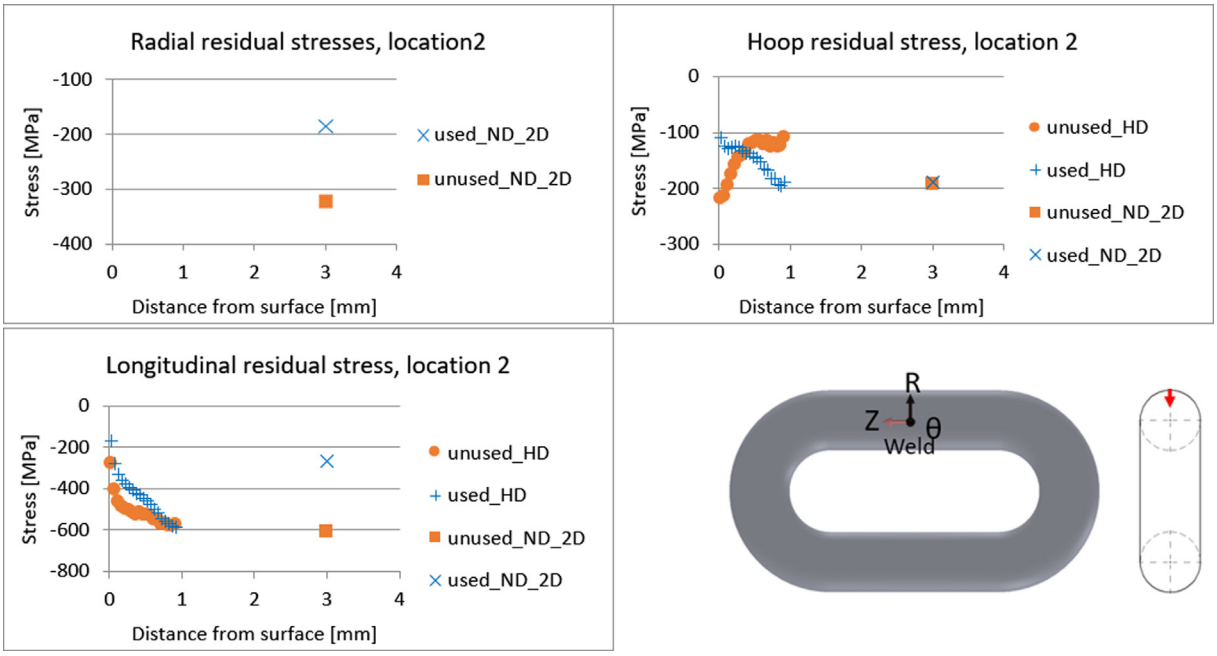

Fig. 5. Comparison of residual stresses measured at the weld part of the chains (location 2) using the HD and ND techniques, the ND results with no radial strain measurement ($\varepsilon_r = 0$) have a _2D suffix; the red arrow indicates measurement location. (For interpretation of the references to colour in this figure legend, the reader is referred to the web version of this article.)

- The RS are compressive in all three measurement directions in both chain links.
- The radial and hoop RS, measured by the ND technique, are approximately 1/2 of the longitudinal RS.
- The unused link has smaller RS, measured by the ND technique, in all three directions. This was opposite in the weld region (location 2).

Due to the beamtime access limitation, in this location, the calculation of the RS in the ND technique is based on a 2-axis measurement (hoop and longitudinal) and thus, the radial strain was set to zero.

Looking at the RS measured inside the straight part (location 4) of the chain links presented in Fig. 8. The application of the HD technique in this location was not possible due to limited space between the two straight parts of the links. From Fig. 8, it is seen that:

- The near-surface RS on the unused link are smaller. This was opposite in the weld region (location 5).
- The radial RS are approximately 1/3 and hoop RS are about 1/2 of the longitudinal RS.
- The RS gradients in the used link are opposite to them at location 5. Thus, in the weld part, faster crack initiation and slower (or even trapped) crack growth is expected, while in the straight part, slower crack initiation with a faster crack growth could occur.

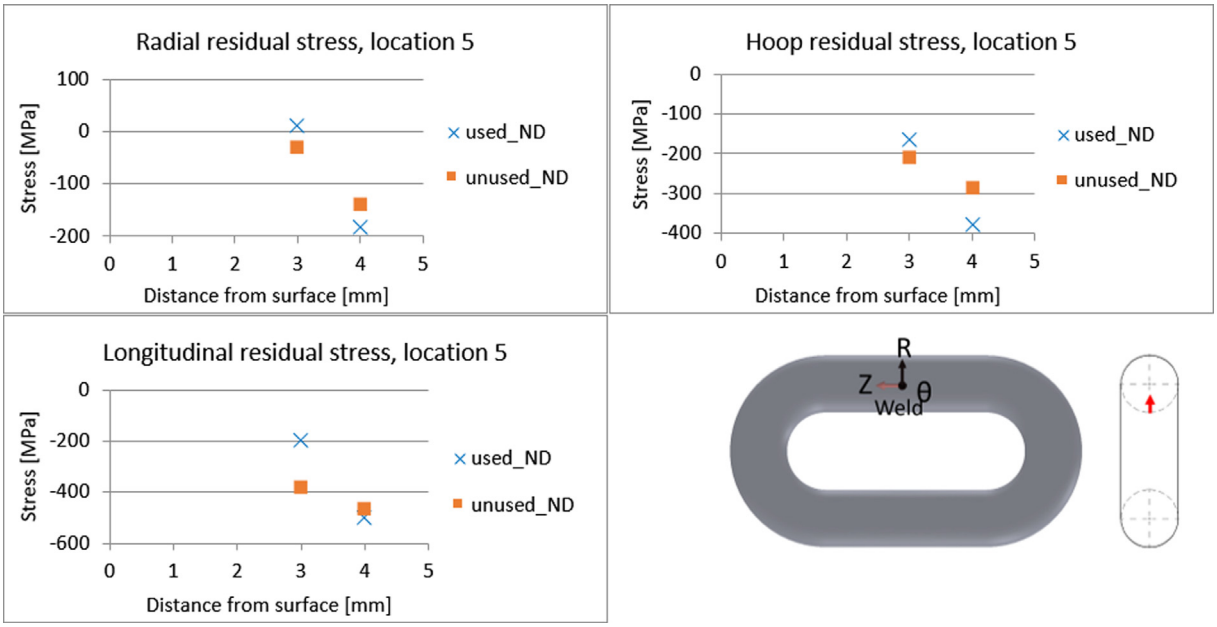

Fig. 6. Comparison of residual stresses measured at the weld part of the chains (location 5) using the ND technique; the red arrow indicates measurement location. (For interpretation of the references to colour in this figure legend, the reader is referred to the web version of this article.)

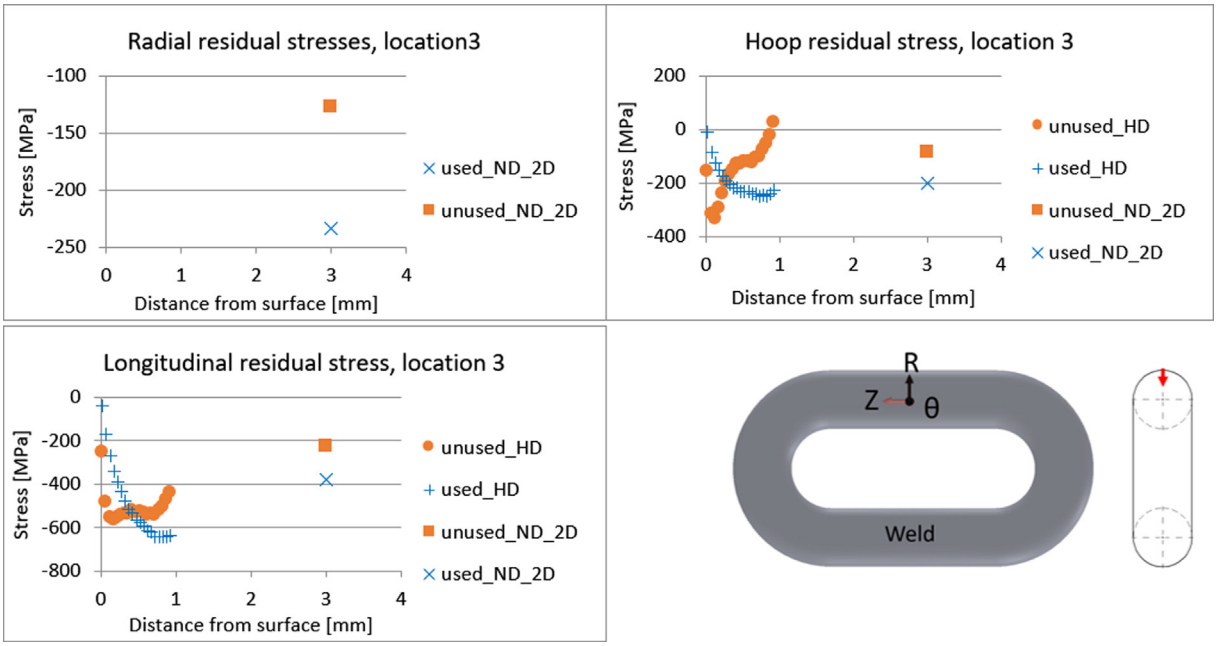

Fig. 7. Comparison of residual stresses measured at the straight part of the chains (location 3) using HD and ND techniques; the red arrow indicates measurement location. (For interpretation of the references to colour in this figure legend, the reader is referred to the web version of this article.)

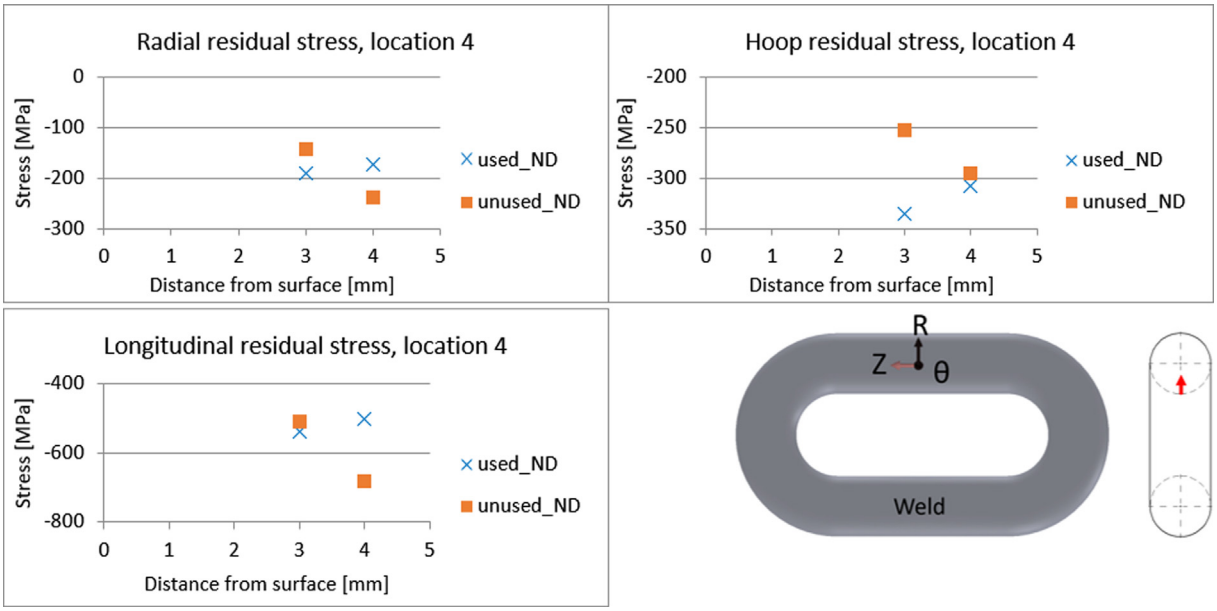

Fig. 8. Comparison of residual stresses measured at the straight part of the chains (location 4) using the ND technique; the red arrow indicates measurement location. (For interpretation of the references to colour in this figure legend, the reader is referred to the web version of this article.)

- The RS gradients in the used chain link are less steep, and in opposite direction, compared to the unused link.

4. Finite element simulation of pitted mooring chains

A model consisting of one complete chain link ($D = 114\ mm$) and two half links is constructed. To reduce the computational efforts, only 1/8 portion of the model with three symmetry planes (XY, YZ, XZ) are used in the analysis, as shown in Fig. 9. Hard contact with standard constraint enforcement method and a stiffness scale factor of 0.01 is applied to the chains' contact regions. A friction coefficient of 0.3 is used for the tangential behavior of the interaction [31]. First-order hexahedral elements with reduced integration schemes (C3D8R) are used, and mesh convergence has been carried out with a finer mesh close to the surface in order to capture RS gradient optimally. The mesh study has been presented in [19]. The material model used in this study combines kinematic and isotropic hardening based on Armstrong-Frederick and Voce parameters, respectively, and is applied in Abaqus software to study the RS redistribution at the pit sites on chain links during the service life (as described and calibrated in [19]). The parameters for the cyclic plasticity analysis of mooring chain steel grade R4 are calibrated such that the material model can simulate both transient and stabilized material response; the parameters are listed in Table 2. Using the calibrated parameters, the stress-strain curve in the first quarter of the first cycle resembles the stress-strain curve from the tensile test. Also note that R4 steel has similar behavior in tension and compression and shows a large cyclic softening response [19].

The proof load (PL) is defined as 70% of the minimum breaking load

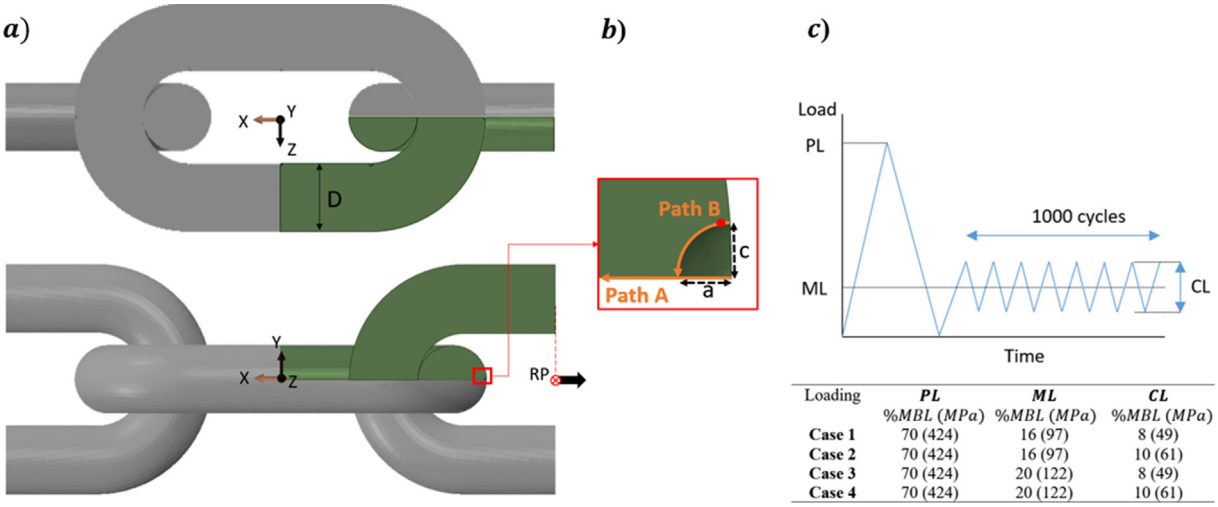

Loading	PL	ML	CL
	%MBL (MPa)	%MBL (MPa)	%MBL (MPa)
Case 1	70 (424)	16 (97)	8 (49)
Case 2	70 (424)	16 (97)	10 (61)
Case 3	70 (424)	20 (122)	8 (49)
Case 4	70 (424)	20 (122)	10 (61)

Fig. 9. (a) Finite element model of chain links with the considered 1/8 of the entire volume (shaded), (b) details of the modeled corrosion pit with the critical point (solid circle), and (c) details of the applied nominal loads.

Table 2
Parameters for combined kinematic with isotropic hardening model identified for the mooring chain steel grade R4 [19].

σ_0 [MPa]	Q_∞ [MPa]	b	c [MPa]	γ
546	−227	3.1	536,565	1500

($MBL = 12420\ \ KN$) [8]. The load is applied at a reference point (RP) which has restricted degrees of freedom (DOFs) in all directions except along the loading axis, i.e. X-axis. The DOFs of the half-chain cross-sections (loaded faces) at the straight parts are kinematically coupled to DOFs of the RP except along the Y-axis. To investigate the effect of corrosion pits on the RS redistribution, a hemispherical pit with 4 mm depth ($a = 4\ \ mm$) and aspect ratio ($a/2c$) of 0.5 is introduced to the model after proof load removal using model change interaction in Abaqus/standard. The modeled pit is located at the chain crown where fatigue cracks are frequently observed [9,32,33]. Subsequently, nominal service loads (the force applied on the cross-section area of the straight parts of a chain link) are applied at the RP. The service load includes a mean load (ML) and a cyclic load (CL) caused by wind, wave, and current. In this study, different service load levels based on what typical mooring chains experience during their service lives are used to investigate the RS redistribution in a pitted studless mooring chain link during its service life. Note that the cyclic load levels correspond to extreme storm situations and the load levels employed in large-scale testing in order to have manageable test durations. Only tension-tension fatigue is considered. Also note that despite the chains being globally load controlled, the loading condition at the pit site can be assumed to be strain-controlled as the plastic zone at the pit site is fairly constrained by the elastic material around it. The loading and boundary conditions are presented in Fig. 9c and Fig. 9a respectively. The FE results are presented for two paths at the chain crown, shown in Fig. 9b.

The FEM predictions of the initial state of RS (right after the proof load removal) and the experimental measurements at the crown are presented in Fig. 10. It is seen that the FE modeling of proof loading alone cannot predict the radial and hoop in-depth RS properly, as there can be some RS in the material from the heat treatment process that is carried out before proof loading. These RS are due to nonhomogeneous plastic deformation caused by different heating/cooling times of the material at the surface and in the core of chain rods. They appear in all three principal directions defined herein, however, the longitudinal RS are later replaced by greater RS from proof loading. The close agreement between the FEM predictions and the measurements of longitudinal RS supports this statement. Well-predicted longitudinal RS, which are also the largest in magnitude, are important when fatigue crack growth is of interest as these stresses are normal to the crack faces commonly observed in the fractured chain links.

The RS redistribution due to corrosion pitting and cyclic straining at the pit site is investigated at the chain crown. The computed distribution of longitudinal RS along path A (starting from the outside of the chain crown towards the contact point) before and after 1000 service load cycles are presented in Fig. 11. It is seen that the material removal due to corrosion is not the main reason for the RS redistribution. Instead, the stress concentration because of the presence of the pit results in cyclic straining at the pit site ending up with a significant local change in the longitudinal RS at the bottom of the pit. In the case studied here, the stress concentration around the modeled pit resulted in introduction of higher compressive RS at the pit tip. This is also seen in the RS measured by the ND technique at this region, see Fig. 10, where more compressive RS were measured at a shallower depth in the used link (i.e. closer to the real corrosion pits at the chain link surface). This change is influenced by the load range (i.e. higher compressive RS as a result of a higher applied load range) but not by the mean load.

The longitudinal RS are compressive up to $40mm$ below the chain outer surface at the crown. However, the superposition of the longitudinal stress due to service loads and RS becomes tensile at a much shorter distance from the surface, see Figs. 12 and 13. One should note that the overall longitudinal stress remains tensile up to half-diameter of the chain. This is important to fatigue crack growth analysis as this tensile stress will facilitate the crack growth.

Fatigue crack initiation lives of the modeled chain links with a corrosion pit for different loading cases are estimated using the multiaxial fatigue criterion described in Section 2.3. $\Delta\gamma_{max}/2$ and $\sigma_{n,max}$ are computed using the principal stresses and principal strains at the critical point extracted from the FEM results. Cyclic elastic–plastic strain analysis of pitted mooring chains has identified a point located on the pit wall and just below the pit mouth, in which accumulated plastic strain is maximum, as the critical point from the fatigue initiation point of view [19]. This critical point is shown in Fig. 9b. Comparison of the estimated lives in Table 3 based on the strain and stress values at this point and a point at the bottom of the pit confirms that fatigue cracks initiate from the identified critical point on the pit wall. Hence, attention will be paid to this critical point for the rest of this article. Three scenarios are considered; first, the RS are neglected (i.e. a non-proof loaded chain link), second, the initial RS state (right after proof load removal) are considered to remain unchanged during the fatigue process, and third, the stable RS state (RS after 1000 cycles of service load)

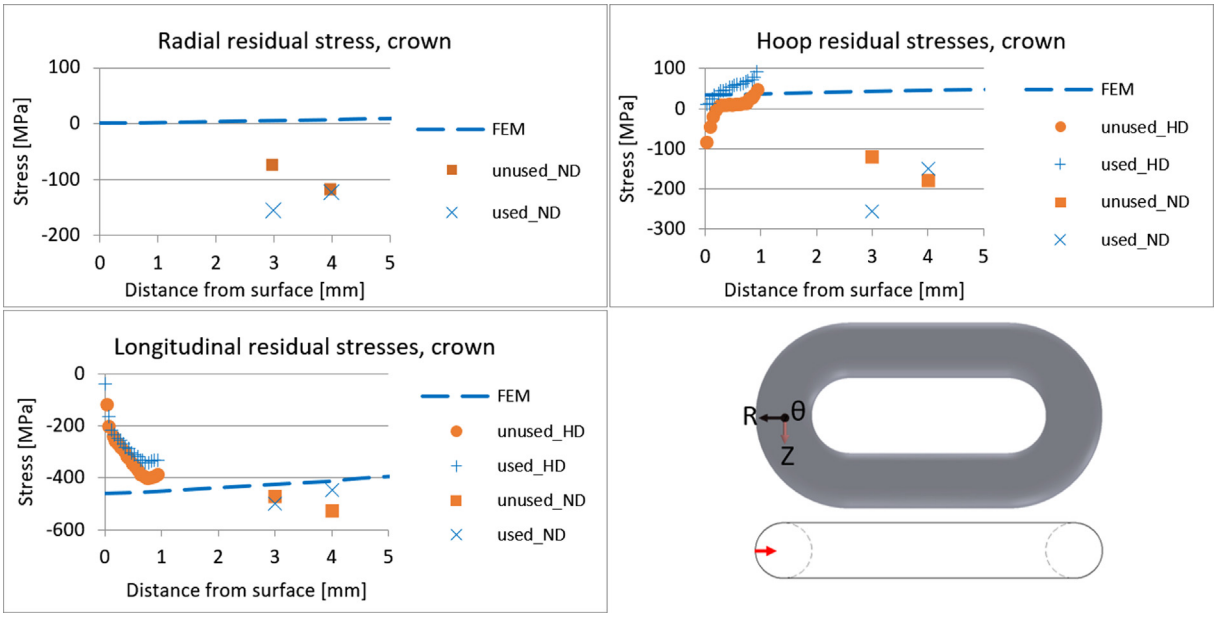

Fig. 10. Comparison of residual stresses measured at the chains' crowns using HD and ND techniques with FEM predictions.

are employed for fatigue life estimation. The estimated fatigue crack initiation lives using Eq. (3) are presented in Table 4. Very short lives are predicted for the non-proof loaded chain link as the effect of high compressive RS is neglected. This was also observed in the fatigue test carried out on the small lifting chains, where the non-proof loaded chains had significantly shorter lives than the proof loaded chains [34]. The estimated lives for the proof loaded chain link with the RS taken directly after proof load removal are 30% shorter (more conservative) than the case where the stable RS were used in the calculations.

The experimental fatigue lives of the corroded chain links ($D = 114\ \ mm$, grade R4) tested in simulated seawater in the lab (3.5% sodium chloride) and predictions using S-N curves presented in DNVGL-OS-E301 [8] are also provided in Table 4. In the large-scale tests, the failure was defined as a through thickness crack. The estimated crack initiation life considering the stable RS state is about 14 to 34% of the experimental (total) life depending on the applied load. It is seen that the load amplitude has a larger effect than the mean load on the fatigue crack initiation life of pitted chains subjected to the loading cases studied here. For example, comparing loading case 1 with 3, a 25% increase in the mean load at the load amplitude of 8% MBL resulted in a 15% decrease in the predicted crack initiation life while comparing loading case 1 with 2, a 25% increase in the load amplitude made the initiation life 75% shorter. The effect of the mean load is more pronounced at lower load amplitudes. It is worth noting that unlike the DNVGL S-N curve in predicting total fatigue lives, this approach can account for the effect of the mean load as well as the load amplitude on the fatigue crack initiation life of pitted mooring chains.

5. Discussion

It must be noted that measuring RS at the surface of a component using the HD technique is challenging, as in this technique RS are calculated using the measured released strains by strain gauges after each drilling increment and since at the first few increments these strains are very small, the corresponding calculated RS are small as well. This can be seen in almost every RS measured by this technique. Hence, the calculated RS may not represent the actual RS at the component surface. Therefore, the authors recommend taking the average value of the measurements in the second half of the hole depth to be representative for the RS at this half.

The complete picture of the RS in the material measured by the ND technique is essential when investigating crack growth considering crack closure. This is the case in fatigue analysis of mooring chains due to high compressive RS. The HD technique is an approach that provides in-plane RS measurement only while the ND technique gives a 3D measurement. The results from ND tests show that there are considerable radial RS (in the order of 1/3 of the maximum absolute residual strain at every point of investigation) inside the chain links (both used and unused). These RS, which are mainly from the manufacturing process, are not captured by the HD technique. As a result, the RS calculated from the 2D strain measurement do not represent the actual 3D RS in the chain material. For the sake of comparison, the radial residual strains measured in the ND technique are set to zero in Equation (1) and the hoop and longitudinal RS at the chain crown are calculated correspondingly. The results are presented in Fig. 14. It is seen that the longitudinal and hoop RS calculated based on the 3D strain measurement are, respectively, 10 and 25% greater than those

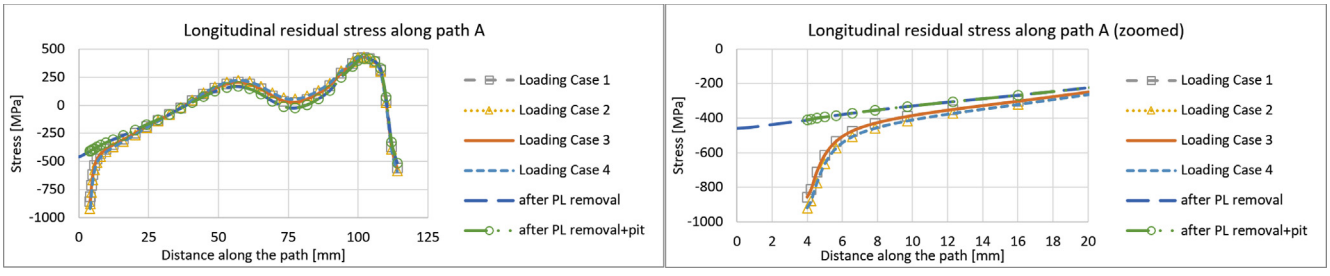

Fig. 11. FE results, longitudinal residual stresses distribution along path A at the crown after proof load removal and after 1000 cycles of different service loads.

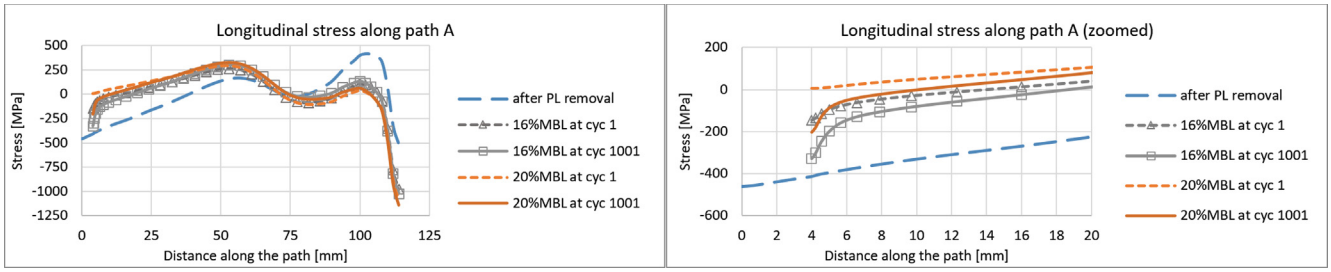

Fig. 12. FE results, longitudinal stress distribution along path A at the crown at the mean load of 16 and 20% MBL before and after 1000 cycles of loading cases 1 and 3 respectively.

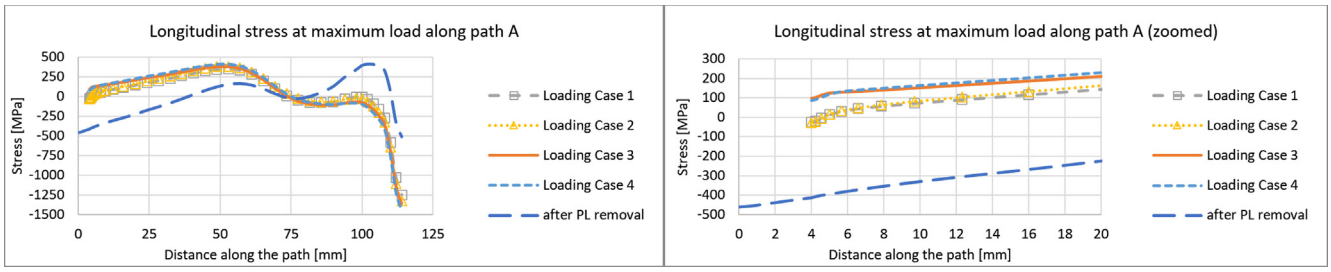

Fig. 13. FE results, longitudinal stress distribution along Path A at the crown at the maximum load at different loading cases after 1000 load cycles.

Table 3
Estimated crack initiation lives based on the stress and strain values at the pit bottom and critical point on the pit wall.

	Pit bottom			Critical point on the pit wall		
Loading	$\sigma_{n,max}$ [MPa]	$\Delta\gamma_{max}/2$	**Cycles**	$\sigma_{n,max}$ [MPa]	$\Delta\gamma_{max}/2$	**Cycles**
Case 1	−1	0.00397	194,682	−39	0.00414	169,440
Case 2	−15	0.00495	52,429	−29	0.00517	43,206
Case 3	51	0.00396	163,397	15	0.00412	143,833
Case 4	44	0.00494	45,357	8	0.00515	40,173

calculated based on the 2D strain measurements. Nevertheless, if the purpose of an experiment is to qualitatively compare the RS in two mooring links, e.g. redistribution/change of RS over a service time, the HD technique could be used as a cheap and relatively quick alternative.

From the fatigue perspective, the FE predictions of RS considering PL only are on the safe side as it predicts zero radial RS instead of the actual compressive RS just below the surface of the chain crown, see Fig. 10. Alternatively, an enhanced FE model that takes the heat treatment process into account may provide a better prediction of RS in the radial directions. However, to account for this, the material properties at elevated temperatures need to be characterized.

The Fatemi-Socie multiaxial damage parameter combined with Roessle-Fatemi hardness method is an efficient method for fatigue life estimations while hardness and yield stress are the only material parameters required. Further, it provides life estimations in the applications, in which large compressive RS present in the material. The Dang Van criterion [36] gives very conservative life estimations in such a condition [10] and the Smith-Watson-Topper parameter [37] fails to predict fatigue life when the maximum stress normal to the crack plane is compressive.

The estimated lives presented in Table 4 show how different the predictions can be depending on the choice of the RS state used in the fatigue life calculation. The important role of RS on fatigue life is well accepted and thus, neglecting RS does not seem to be a reasonable choice. For simplicity, one could use the initial RS state in the fatigue crack initiation and growth models. However, it should be noted that the fatigue life estimation criteria that do not account for the RS redistribution lead to incorrect (generally more conservative) remaining life predictions, as RS change cycle by cycle as a result of cyclic plastic straining at the tip of a growing pit/crack even though the nominal load is below the materials yield limit.

In this study, different service load levels corresponding to extreme storm situations and the load levels employed in large-scale testing were studied. However, the approach is general, and a more detailed loading condition (e.g. considering several sea states) can be used in the simulation. The maximum shear strain range and the maximum normal stress on the maximum shear strain plane for each sea state can be obtained from FE simulation and using e.g. Palmgren-Miner rule, one can estimate the crack initiation life of a pitted chain link subjected to a more typical loading condition. However, the sea state data at the specific geographical location of the offshore vessel under study is required for such an assessment.

Table 4
Stress and strain values at the critical point on the pit wall, the estimated crack initiation life, and experimental total life.

	N_f *experimental*	N_f *DNVGL*	Non-proof loaded link			Proof loaded link, initial RS state			Proof loaded link, stable RS state		
Loading	**Cycles**	**Cycles**	$\sigma_{n,max}$ [MPa]	$\Delta\gamma_{max}/2$	**Cycles**	$\sigma_{n,max}$ [MPa]	$\Delta\gamma_{max}/2$	**Cycles**	$\sigma_{n,max}$ [MPa]	$\Delta\gamma_{max}/2$	**Cycles**
Case 1	501,872*	520,436	488	0.00498	18,348	53	0.00417	116,585	−39	0.00414	169,440
Case 2	318,174*	266,430	496	0.00616	8,035	92	0.00528	29,044	−29	0.00517	43,206
Case 3	–	520,436	500	0.00491	19,102	132	0.00413	96,976	15	0.00412	143,833
Case 4	126,614**	266,430	502	0.00620	7,795	171	0.00516	27,434	8	0.00515	40,173

* Reported by Fredheim et al. in [35].
** Unpublished report.

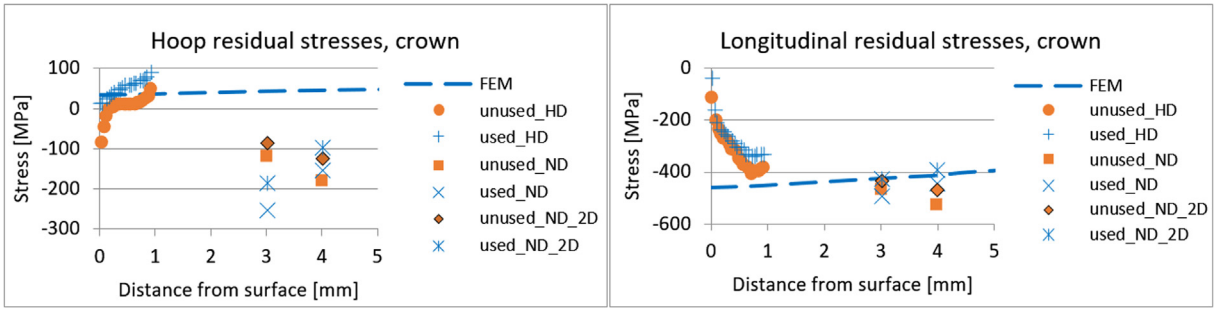

Fig. 14. Residual stresses at the crown, the ND results with $\varepsilon_r = 0$ have a 2D suffix.

6. Conclusion

Residual stresses (RS) in offshore mooring chains have been measured for the first time. Two chain links with the same size and material, one only subjected to proof load and no cyclic service loads (herein referred to as the unused link) and the other exposed to service loads as well as the proof load (herein referred to as the used link), were selected for the experiment to investigate RS changes over the service life. The RS just below the surface were measured using the hole the drilling (HD) technique and the neutron diffraction (ND) technique has been employed for deeper measurements. Finite element (FE) simulation of the proof loading as well as cyclic service loads has been done to investigate the RS redistribution around a typical corrosion pit at the chain surface. The results were compared with the experimental measurements of RS. Further, the Fatemi-Socie multiaxial damage parameter combined with Roessle-Fatemi hardness method was employed to estimate fatigue crack initiation life of pitted mooring chains at various service load levels considering the effect of residual stresses. The key findings are:

- Both the HD and ND techniques have revealed the existence of high compressive RS in all measurement points with the longitudinal RS being the largest in magnitude. An exception was seen on the hoop RS measured by the HD technique at the crown where the RS were tensile.
- The radial RS that cannot be measured using the HD technique are rather considerable (approximately 25 to 50% of the longitudinal RS). The ND technique provides the measurement of the radial RS due to its capability of 3D residual strain measurement.
- Comparison of the RS at the crown calculated using the ND technique and based on 3D strain measurements with those calculated based on 2D strain measurements, where radial residual strain is set to zero, revealed 10 and 25% greater longitudinal and hoop RS respectively in the 3D calculation. This highlights the importance of 3D strain measurements in RS calculation. The HD technique is an approach that provides in-plane RS measurement only. As a result, the measurement made by this technique will not be the most accurate when the residual strains normal to the surface are considerable. Nevertheless, if the purpose of an experiment is to qualitatively compare the RS in two links to investigate the redistribution/change of RS over a service time, the HD technique could be used as a cheap and relatively quick alternative.
- The longitudinal RS (which are the largest in magnitude) at the chain crown predicted by FE modeling of proof loading are in a good agreement with the experimental measurements. Well-predicted longitudinal RS are important when fatigue crack growth is of interest as these stresses are normal to the crack faces commonly observed in the fractured chain links. The predicted radial and hoop RS are different from the in-depth measured values, as there can be some RS in the material from the heat treatment process that is carried out before proof loading. A more detailed FE model can be employed to better estimate the radial RS by considering the heat treatment process. However, the material properties at elevated temperatures are needed.
- The RS redistribution due to a corrosion pit and cyclic service loads has been studied. The redistribution of the RS has been explained by the stress concentration and cyclic plastic straining around corrosion pits that replaces the initial RS with greater RS. A current RS state can locally differ significantly from an initial RS state. This is important when the fatigue crack initiation and growth is to be studied.
- Very short crack initiation lives were predicted for the non-proof loaded chain link (i.e. no RS considered). The lives predicted for the proof loaded chain link in the cases where the initial RS state was used in the calculations were 30% shorter (more conservative) than the cases where the stable RS state was employed. The predicted crack initiation lives considering the stable RS state is about 14 to 34% of the experimental (total) life depending on the applied load. Further, the effect of mean load on the fatigue life has been successfully captured. This effect is larger when the load amplitude is smaller.

Declaration of Competing Interest

The authors declare that they have no known competing financial interests or personal relationships that could have appeared to influence the work reported in this paper.

Acknowledgement

The authors would like to acknowledge Equinor for providing the test material and financially supporting the experiments through the project KPN Lifemoor (RCN contract No: 280705), Øystein Gabrielsen (Equinor) and Håkon Nordhagen (SINTEF) for help and discussion throughout the research process, SINTEF laboratory staffs for their assistance in performing the hole-drilling tests, and Rutherford Appleton Laboratory for granting the access to ENGIN-X and neutron beamtime. Also, the initial discussions and facilitation for ND testing with assoc prof Stephen Hall (Lund University, Solid Mechanics) are acknowledged.

References

[1] Fontaine E, et al. Industry survey of past failures, pre-emptive replacements and reported degradations for mooring systems of floating production units, in offshore technology conference. Offshore technology conference. 2014.
[2] Ma, K.-t., et al., A Historical Review on Integrity Issues of Permanent Mooring Systems, in Offshore Technology Conference. 2013, Offshore Technology Conference.
[3] Apos, Souza R, Majhi S. Application of lessons learned from field experience to design, installation and maintenance of FPS moorings, in offshore technology conference. Offshore technology conference. 2013.
[4] ISO19901-7:2013. Stationkeeping systems for floating offshore structures and mobile offshore units, in part 7 of Petroleum and natural gas industries specific requirements for offshore structures.
[5] DNVGL. Offshore standard DNV-OS-E302 offshore mooring chain; 2015, DNV GL AS.

[6] Totten GE. Handbook of residual stress and deformation of steel. ASM International; 2002.
[7] Bastid P, Smith SD. Numerical analysis of contact stresses between mooring chain links and potential consequences for fatigue damage. ASME 2013 32nd international conference on ocean, offshore and arctic engineering. American Society of Mechanical Engineers; 2013.
[8] DNVGL. Offshore standard DNVGL-OS-E301 Position mooring; 2015, DNV GL AS.
[9] Gabrielsen Ø, Larsen K, Reinholdtsen S-A. Fatigue testing of used mooring chain. ASME 2017, 2017(57632). p. V001T01A072.
[10] Perez IM, et al. Multiaxial fatigue analysis of mooring chain links under tension loading: Influence of mean load and simplified assessment. ASME 2018 37th international conference on ocean, offshore and arctic engineering. American Society of Mechanical Engineers; 2018.
[11] Pérez-Mora R, et al. Very high cycle fatigue of a high strength steel under sea water corrosion: A strong corrosion and mechanical damage coupling. Int J Fatigue 2015;74:156–65.
[12] Stiff JJ, Smith DW, Casey NF. Fatigue of mooring chain in air and water - results and analysis, in offshore technology conference. Offshore technology conference; 1996.
[13] Huang Y, Tu S-T, Xuan F-Z. Pit to crack transition behavior in proportional and non-proportional multiaxial corrosion fatigue of 304 stainless steel. Eng Fract Mech 2017;184:259–72.
[14] Huang Y, et al. Numerical investigation of stress concentration factor at irregular corrosion pit under tension-torsion loading. ASME 2014 pressure vessels and piping conference. American Society of Mechanical Engineers; 2014.
[15] Turnbull A, Horner DA, Connolly BJ. Challenges in modelling the evolution of stress corrosion cracks from pits. Eng Fract Mech 2009;76(5):633–40.
[16] Horner DA, et al. Novel images of the evolution of stress corrosion cracks from corrosion pits. Corros Sci 2011;53(11):3466–85.
[17] Xu S-H, Wang Y-D. Estimating the effects of corrosion pits on the fatigue life of steel plate based on the 3D profile. Int J Fatigue 2015;72:27–41.
[18] Turnbull A, Wright L, Crocker L. New insight into the pit-to-crack transition from finite element analysis of the stress and strain distribution around a corrosion pit. Corros Sci 2010;52(4):1492–8.
[19] Zarandi EP, Skallerud BH. Cyclic behavior and strain energy-based fatigue damage analysis of mooring chains high strength steel. Mar struct 2020;70:102703.
[20] Fatemi A, Socie DF. A critical plane approach to multiaxial fatigue damage including out-of-phase loading. Fatigue Fract Eng Mater Struct 1988;11(3):149–65.
[21] Roessle ML, Fatemi A. Strain-controlled fatigue properties of steels and some simple approximations. Int J Fatigue 2000;22(6):495–511.
[22] Lee TL, et al. Characterization of the residual stresses in spray-formed steels using neutron diffraction. Scr Mater 2015;100:82–5.
[23] Bouchard P, et al. Measurement of the residual stresses in a stainless steel pipe girth weld containing long and short repairs. Int J Press Vessels Pip 2005;82(4):299–310.
[24] Hossain S, et al. Application of quenching to create highly triaxial residual stresses in type 316H stainless steels. Int J Mech Sci 2006;48(3):235–43.
[25] Abolfathi E, et al. The effect of the manufacturing test load on the fatigue of hoist chains. Proc Inst Mech Eng, Part B: J Eng Manuf 1995;209(2):133–9.
[26] ASTM, E837-13, standard test method for determining residual stresses by the hole-drilling strain-gage method; 2013.
[27] MTS3000-RESTAN, System for measureing residual stress by hole-drilling method, EVAL back calculation software. 2015, SINT Technology: Italy.
[28] Shamsaei N, McKelvey SA. Multiaxial life predictions in absence of any fatigue properties. Int J Fatigue 2014;67:62–72.
[29] Shamsaei N, Fatemi A. Effect of hardness on multiaxial fatigue behaviour and some simple approximations for steels. Fatigue Fract Eng Mater Struct 2009;32(8):631–46.
[30] Zarandi E, Lee T, Skallerud B. Data on residual stresses of mooring chains measured by neutron diffraction and hole drilling techniques. Data in Brief, under revision; 2019.
[31] Rampi L, et al. Chain out of plane bending (OPB) fatigue joint industry project (JIP) static test program and OPB interlink stiffness. ASME 2016 35th international conference on ocean, offshore and arctic engineering. American Society of Mechanical Engineers; 2016.
[32] Fernández J, Storesund W, Navas J. Fatigue performance of grade R4 and R5 mooring chains in seawater. ASME 2014 33rd international conference on ocean, offshore and arctic engineering. American Society of Mechanical Engineers; 2014.
[33] Brown M, et al. SS: mooring system integrity: phase 2 mooring integrity JIP - summary of findings, in offshore technology conference. Offshore technology conference; 2010.
[34] Tipton S, Shoup G. The effect of proof loading on the fatigue behavior of open link chain. J Eng Mater Technol 1992;114(1):27–33.
[35] Fredheim S, et al. Corrosion fatigue testing of used, studless, offshore mooring chain. OMAE2013-10609. Nantes: 32nd international conference on ocean, offshore and arctic engineering. 2013.
[36] Van KD, et al. Criterion for high-cycle fatigue failure under multiaxial loading. ICBMFF2. 1989.
[37] Smith R, Watson P, Topper T. A stress-strain parameter for the fatigue of metals. J Mater 1970;5(4):767–78.